Sr_3MCrO_6 (M = Sc, In, Lu, Yb, Tm, Er, Ho, Y): The First Chromium-Containing $A_3A'BO_6$ Oxides

Mark D. Smith and Hans-Conrad zur Loye*

Department of Chemistry and Biochemistry, University of South Carolina, Columbia, South Carolina 29208

Received January 31, 2000. Revised Manuscript Received May 15, 2000

The first chromium-containing members of the $A_3A'BO_6$ family of pseudo-one-dimensional oxides, Sr_3MCrO_6 (nominal composition; M = Sc, In, Lu, Yb, Tm, Er, Ho, Y), have been synthesized by stoichiometric reaction of SrO, Cr_2O_3, and M_2O_3 in sealed fused silica tubes at 1050 °C for 24 h. The compounds required anaerobic preparation conditions because of the oxidative instability of Cr^{3+} in these systems. Sr_3MCrO_6 adopt the K_4CdCl_6 structure type, consisting of $^1_\infty[MO_{6/2}CrO_{6/2}]$ metal−oxygen polyhedral chains composed of alternating face-shared Sc, In, Y, or rare-earth MO_6 trigonal prisms and CrO_6 octahedra. The metal−oxygen polyhedral chains are surrounded by columns of Sr^{2+} cations. The compounds obey the Curie−Weiss law at higher temperatures. All were structurally characterized by powder X-ray diffraction. The synthesis, structural determination, and magnetic behavior of these oxides is discussed.

Introduction

Recently there has been a great deal of interest in a family of pseudo-one-dimensional oxides derived from the K_4CdCl_6 structure type[1] with the formula $A_3A'BO_6$ (A = Ca, Sr, Ba; A′/B = $A'^{+}/B^{5+,2-4}$ $A'^{2+}/B^{4+,5-10}$ $A'^{3+}/B^{3+,11,12}$ A'^{4+}/B^{2+} [13]). Work by various groups has resulted in a variety of compositions as well as in detailed structural and magnetic property determinations. Investigation into the nature of the magnetism of these oxides has proven particularly rewarding because of their highly anisotropic structures, and phenomena such as ferromagnetism,[14,15] antiferromagnetism,[7,14,16−17] and more complex magnetic behavior[18−20] have been uncovered. The $A_3A'BO_6$ family can be viewed as composite oxides consisting of two mutually interpenetrating one-dimensional subsystems, one based on columns of A^{2+} cations and the other based on chains of alternating, face-shared metal−oxygen $A'O_6$ trigonal prisms and BO_6 octahedra, both running along the hexagonal [001] direction. It is important to point out that compounds of the $A_3A'BO_6$ type are actually members of a much larger family of commensurately and incommensurately modulated structures, which differ in the sequence and ratio of BO_6 octahedra and $A'O_6$ trigonal prisms in the chains. Systematic treatments unifying the various compositions have been advanced by different authors.[21−25] Previous reports of $A_3A'BO_6$ and closely related oxide systems containing a first-row transition metal on the octahedral "B" site have incorporated metals as far left in the first transition series as Mn^{4+} in the phases Ca_3MMnO_6 (M = Ni, Zn).[19] The structurally related $Ba_6MMn_4O_{15}$ (M = Cu, Zn, Pd) are also known.[26,27] Proceeding one element

* To whom correspondence should be addressed. E-mail: zurloye@sc.edu.

(1) Bergerhoff, G.; Schmitz-Dumont, O. *Z. Anorg. Allg. Chem.* **1956**, *284*, 10.
(2) Reisner, B. A.; Stacy, A. M. *J. Am. Chem. Soc.* **1998**, *120*, 9682.
(3) Frenzen, S.; Müller-Buschbaum, Hk. *Z. Naturforsch., B: Chem. Sci.* **1996**, *51*, 1204.
(4) Wehrum, G.; Hoppe, R. *Z. Anorg. Allg. Chem.* **1992**, *617*, 45.
(5) Claridge, J. B.; Layland, R. C.; Henley, W. H.; zur Loye, H.-C. *Chem. Mater.* **1999**, *11*, 1376.
(6) Kageyama, H.; Yoshimura, K.; Kosuge, K. *J. Solid State Chem.* **1998**, *140*, 14.
(7) Vente, J. F.; Lear, J. K.; Battle, P. B. *J. Mater. Chem.* **1995**, *5*, 1785.
(8) Tomaszewska, A.; Müller-Buschbaum, Hk. *Z. Anorg. Allg. Chem.* **1993**, *619*, 534.
(9) Wilkinson, A. P.; Cheetham, A. K.; Kunnman, W.; Kvick, Å. *Eur. J. Solid State Inorg. Chem.* **1991**, *28*, 453.
(10) Randall, J. J.; Katz, L. *Acta Crystallogr.* **1959**, *12*, 519.
(11) (a) Núñez, P.; Rzeznik, M. A.; zur Loye, H.-C. *Z. Anorg. Allg. Chem.* **1997**, *623*, 1269. (b) Layland, R. C.; Kirkland, S. L., zur Loye, H.-C. *J. Solid State Chem.* **1998**, *139*, 79. (c) Layland, R. C.; Kirkland, S. L.; Núñez, P.; zur Loye, H.-C. *J. Solid State Chem.* **1998**, *139*, 416.
(12) (a) James, M.; Attfield, J. P. *J. Mater. Chem.* **1994**, *4*, 575. (b) James, M.; Attfield, J. P. *Chem. Eur. J.* **1996**, *2*, 737.
(13) Smith, M. D.; Stalick, J. K.; zur Loye, H.-C. *Chem. Mater.* **1999**, *11*, 2984.
(14) Nguyen, T. N.; zur Loye, H.-C. *J. Solid State Chem.* **1995**, *117*, 300.
(15) Aasland, S.; Fjellvag, H.; Hauback, B. *Solid State Commun.* **1997**, *101*, 187.
(16) Segal, N.; Vente, J. F.; Bush, T. S.; Battle, P. D. *J. Mater. Chem.* **1996**, *6*, 395.
(17) Núñez, P.; Trail, S.; zur Loye, H.-C. *J. Solid State Chem.* **1997**, *130*, 35.
(18) Nguyen, T. N.; Lee, P. A.; zur Loye, H.-C. *Science* **1996**, *271*, 489.
(19) Kawasaki, S.; Takano, M.; Inami, T. *J. Solid State Chem.* **1999**, *145*, 302.
(20) Beauchamp, K. M.; Irons, S. H.; Sangrey, T. O.; Smith, M. D.; zur Loye, H.-C. *Phys. Rev. B.* **2000**, *61*, 11594.
(21) Darriet, J.; Subramanian, M. *J. Mater. Chem.* **1995**, *5*, 543.
(22) Evain, M.; Boucher, F.; Gourdon, O.; Petricek, V.; Dusek, M.; Bezdicka, P. *Chem. Mater.* **1998**, *10*, 3068.
(23) Blake, G. R.; Sloan, J.; Vente, J. F.; Battle, P. D. *Chem. Mater.* **1998**, *10*, 3536.
(24) Perez-Mato, J. M.; Zakhour-Nakhl, M.; Weill, F.; Darriet, J. *J. Mater. Chem.* **1999**, *9*, 2795.
(25) Zakhour-Nakhl, M.; Claridge, J. B.; Darriet, J.; Weill, F.; zur Loye, H.-C.; Perez-Mato, J.-M. *J. Am. Chem. Soc.* **2000**, *122*, 1618.

10.1021/cm000084a CCC: $19.00
Published on Web 07/22/2000

further to the left in the periodic table (to chromium) is accompanied by a significant increase in the ease of oxidation of the metal and therefore in increased difficulty stabilizing the lower (usually +3 or +4) oxidation states normally adopted by the B site atom. However, by employing inert atmosphere synthetic conditions, we have extended the range of the $A_3A'BO_6$ oxides one element to the left of the first transition series with the synthesis of Sr_3MCrO_6 (idealized composition; M = Sc, In, Y, Lu, Yb, Tm, Er, Ho), the first chromium-containing members of this family. The greater electropositivity of chromium relative to the later first-row transition metals manifests itself in the need to synthesize the compounds in vacuo to prevent oxidation of chromium and the formation of chromates. Herein we report the synthesis, structural characterization, and magnetic behavior of Sr_3MCrO_6.

Experimental Section

Sr_3MCrO_6 were synthesized by heating stoichiometric quantities of SrO, Cr_2O_3, and M_2O_3 in vacuo at 1050 °C. All reagent oxides were stored and handled in an Ar-filled glovebox (H_2O + O_2 level < 10 ppm) because of the moisture sensitivity of SrO and M_2O_3. SrO was prepared by thermal decomposition of SrO_2 (Aldrich, 99.9%) or $SrCO_3$ (Aesar, 99.99%) in air at 1150 °C for 48 h. Cr_2O_3 (Baker, 99.96%) and M_2O_3 (Sc_2O_3, Aran Isles Chemicals, 99.99%; In_2O_3, Cerac, 99.99%; Y_2O_3, REacton, 99.99%; Lu_2O_3, Aesar, 99.99%; Yb_2O_3, REacton, 99.99%; Tm_2O_3, Aesar, 99.99%) were dried at 1000 °C in air before introduction into the glovebox. Er_2O_3 and Ho_2O_3 were generated by heating $ErCl_3 \cdot 6H_2O$ (Aesar, 99.99%) and $Ho(NO_3)_3 \cdot 5H_2O$ (Aldrich, 99.9%), respectively, in air at 1000 °C for 24 h. The purity of all starting materials was verified by powder X-ray diffraction before use. The precursor oxides were ground thoroughly and manually packed into an alumina crucible, which was placed in a fused silica tube, evacuated ($\sim 10^{-5}$ Torr), and flame-sealed. The crucibles and the silica tubes were both dried at 1000 °C in vacuo before use. The sealed reaction vessels were then heated in an upright position in a box furnace at 1050 °C for 24 h before quenching in air. The tubes were opened in air, as all products are stable to air and moisture indefinitely. For the M = Y, Lu, Yb, Tm, Er, and Ho samples, a light green crust of an unidentified impurity formed on the outside of the heated pellets. This crust was removed with a file, revealing a brown interior. Sr_3ScCrO_6 and Sr_3InCrO_6 were also light brown in color. The compounds were readily identified by the expected similarity of their X-ray powder diffraction patterns to the many $Sr_3A'BO_6$ oxides prepared in our lab and elsewhere, and were easily indexed in the rhombohedral K_4CdCl_6 structure type ($R\bar{3}c$, $a \sim 9.7$ Å, $c \sim 11$ Å). X-ray powder diffraction data suitable for Rietveld refinements for the samples M = Ho, Er, Tm, and Yb were collected on a Rigaku Dmax 2000 diffractometer operating in Bragg−Brentano geometry, with a step size of 0.02°. Counting times varied with each sample but were adjusted using prescans to yield an I (intensity) = 100% peak of $\sim 10^4$ counts. Data sets for M = Sc, In, Y, and Lu were collected on beamline X7A at the National Synchrotron Light Source (NSLS), Brookhaven National Laboratory. The synchrotron wavelength, 0.7997(1) Å, was calibrated using a CeO_2 standard. The step size used was 0.01° over the angular ranges $6° \le 2\theta \le 66°$, with angle-dependent variable counting times/step as follows: $6 \le 2\theta < 16°$, 20 s; $16 \le 2\theta < 36°$, 40 s; $36 \le 2\theta < 51°$, 80 s; $51 \le 2\theta \le 66°$, 160 s. All data points were then normalized during data processing. Only four samples were collected with synchrotron radiation at the NSLS due to beam time limitations. Using K_4CdCl_6 structural data as an initial model, the data sets for all eight compounds were refined using the Rietveld method,[28] as implemented in the General Structure Analysis System (GSAS) suite of programs.[29] Because of the presence of small amounts of the impurity phase SrM_2O_4 for M = Y, Lu, Yb, Tm, Er, and Ho, two-phase refinements were necessary for these compounds. No evidence for $SrSc_2O_4$ and $SrIn_2O_4$ was observed in the powder patterns for the Sc and In compounds. Initial lattice constants and atomic positions for SrM_2O_4 were taken from the literature data for $SrYb_2O_4$ ($CaFe_2O_4$ type).[30] Subsequently, the lattice constants and metal atomic positional parameters were refined. Scale factors were refined for both phases, yielding the relative Sr_3MCrO_6/SrM_2O_4 concentrations in the bulk samples. This information was later used to interpret the magnetic susceptibility data.

Magnetic susceptibility measurements as a function of temperature (2−300 K) were taken at 5 kOe, using a Quantum Design MPMS superconducting quantum interference device (SQUID) magnetometer. Both zero field-cooled (ZFC) and field-cooled (FC) measurements were performed. The finely powdered samples were contained in gelatin capsules fixed inside plastic straws for immersion into the SQUID. No diamagnetic correction was made for the sample container because its signal was insignificant relative to the samples.

Results and Discussion

Sr_3MCrO_6 form readily from direct reaction of the constituent oxides SrO, M_2O_3, and Cr_2O_3 at 1050 °C in a vacuum of $\sim 10^{-5}$ Torr in sealed fused silica tubes. Reaction times as short as 6 h afford complete conversion of starting materials to the final products, but heating for 24 h yields more highly crystalline material. Stoichiometric reaction of the same starting materials at 1050 °C for 24 h under pure flowing nitrogen does not yield Sr_3MCrO_6, but instead results in SrM_2O_4, Cr_2O_3, and minor unknown phases. This is the first observation of chromium in the intensely studied $A_3A'BO_6$ structural family, though rare earths have been previously observed (occupying the trigonal prismatic A′ site) in Sr_3MRhO_6 (M = Yb − Sm)[11] and in Sr_3MNiO_6 (M = Sc, In, Lu, Yb, Tm, Er).[12] The absence of any chromium-containing $A_3A'BO_6$ oxides until now clearly is not due to any inherent chemical reason preventing stabilization of Cr^{3+} in the structure, but rather because of the need for anaerobic synthetic techniques not routinely applied in high-temperature oxide chemistry. Previous syntheses of other reduced multinary alkaline earth-containing chromium oxides have also demonstrated this point; for example, $Sr_3Cr_2WO_9$ (vacuum),[31] $SrCr_{10}O_{15}$ (H_2/argon),[32] $Sr_4Cr_3O_9$ (argon),[33] and $NdCaCrO_4$ (argon).[34] In fact, the mixed-

(26) Cussen, E. J.; Vente, J. F.; Battle, P. D. *J. Am. Chem. Soc.* **1999**, *121*, 3958.
(27) Battle, P. D.; Burley, J. C.; Cussen, E. J.; Darriet, J.; Weill, F. *J. Mater. Chem.* **1999**, *9*, 479.
(28) Rietveld, H. M. *J. Appl. Crystallogr.* **1969**, *2*, 65.
(29) Larson, A. C.; Von Dreele, R. B. General Structure Analysis System (GSAS); Los Alamos National Laboratory, Report No. LA-UR-86-748, Los Alamos, NM, 1994.
(30) Müller-Buschbaum, Hk.; von Schenk, R. *Z. Anorg. Allg. Chem.* **1970**, *377*, 70.
(31) Ballutaud-Harari, D.; Poix, P. *J. Solid State Chem.* **1975**, *14*, 354.
(32) Cuno, E.; Müller-Buschbaum, Hk. *Z. Anorg. Allg. Chem.* **1989**, *572*, 89.
(33) Cuno, E.; Müller-Buschbaum, Hk. *Z. Anorg. Allg. Chem.* **1989**, *572*, 175.
(34) Romero de Pax, J.; Hernández, Velasco, J.; Fernández-Díaz, M. T.; Martínez, J. L.; Sáez Puche, R. *J. Solid State Chem.* **1999**, *148*, 361.

Table 1. Crystallographic Data and Rietveld Refinement Summary for Sr_3MCrO_6

	M							
parameter	Sc	In	Lu	Yb	Tm	Er	Ho	Y
fw	455.812	525.671	585.820	583.893	579.787	578.113	575.783	499.758
a (Å)	9.6999(1)	9.6951(1)	9.7428(1)	9.7438(3)	9.7419(5)	9.7524(4)	9.7518(4)	9.7561(1)
c (Å)	10.9253(1)	11.1313(1)	11.1716(1)	11.1980(4)	11.2151(6)	11.2469(5)	11.2668(5)	11.2747(1)
vol. (Å^3)	890.23(2)	906.10(2)	918.36(2)	920.73(8)	921.8(1)	926.38(10)	927.90(9)	929.37(2)
c/*a*	1.126	1.148	1.147	1.149	1.151	1.153	1.155	1.156
Wt frac.[a]	1.00	1.00	0.927	0.939	0.900	0.934	0.960	0.949
M s.o.f.[b]	1.00	1.00	0.956	0.912	0.910	0.911	0.804	0.900
R_p	0.0497	0.0625	0.0729	0.0735	0.0628	0.0746	0.0795	0.0741
wR_p	0.0517	0.0724	0.1022	0.1037	0.0840	0.0992	0.1064	0.0833
R_{exp}	0.0121	0.0130	0.0719	0.0739	0.0626	0.0691	0.0750	0.0112
χ^2	18.3	30.9	24.6	1.981	1.901	2.078	2.025	27.3
# Var.	20	21	36	36	36	36	36	36

[a] Weight fraction $Sr_3(M_{1-x}Cr_x)CrO_6$ in the Rietveld sample. Impurity phase: SrM_2O_4. [b] M-position site occupation factor; $x = (1 - \text{M s.o.f.})$.

Table 2. Atomic Positions and Isotropic Thermal Parameters for Sr_3MCrO_6[a]

	M							
parameter	Sc	In	Lu	Yb	Tm	Er	Ho	Y
				Sr				
x	0.36585(5)	0.36594(6)	0.36632(8)	0.3633(1)	0.3665(1)	0.3666(1)	0.3664(1)	0.36642(7)
				Oxygen				
x	0.1682(2)	0.1744(3)	0.1740(4)	0.1729(4)	0.1731(5)	0.1742(5)	0.1750(4)	0.1732(3)
y	0.0189(2)	0.0219(3)	0.0203(5)	0.0205(5)	0.0201(6)	0.0194(6)	0.0222(5)	0.0206(4)
z	0.1153(2)	0.1116(3)	0.1118(4)	0.1114(3)	0.1114(4)	0.1104(4)	0.1089(4)	0.1089(3)
				100 x U_{iso}				
Sr	0.26(1)	0.59(1)	0.67(2)	0.82(3)	0.70(4)	0.37(4)	0.60(4)	0.61(2)
M	0.40(3)	0.65(2)	0.50(2)	0.56(4)	0.67(6)	0.35(6)	0.77(6)	0.44(3)
Cr	0.62(3)	0.65(4)	0.79(5)	0.70(8)	0.65(10)	0.20(10)	0.74(9)	0.83(4)
O	0.89(6)	1.48(8)	1.5(1)	0.6(1)	0.7(1)	0.4(1)	0.6(1)	1.35(8)

[a] General: Sr, (*x*, 0, 1/4); M (0, 0, 1/4); Cr, (0 0 0); O, (*x*, *y*, *z*).

valent compound $Sr_4Cr_3O_9$ possesses a pseudo-one-dimensional structure similar to the $A_3A'BO_6$ oxides, containing chains of distorted face-shared Cr−O polyhedra, and may be considered a distant structural relative of the $A_3A'BO_6$ family.[21]

Sr_3ScCrO_6 and Sr_3InCrO_6 could be prepared phase-pure; however, for M = Y, Lu, Yb, Tm, Er, and Ho, a small amount of the impurity phase SrM_2O_4 was always observed (maximum concentration, ~16 mol % in the Yb sample, according to the Rietveld refinements). Sr_3MCrO_6 and SrM_2O_4 apparently exist in equilibrium with one another, as no amount of in vacuo annealing of Sr_3MCrO_6/SrM_2O_4 mixtures resulted in any change in the relative intensities of the X-ray diffraction peaks due to each phase. Based on composition information gained from the refinements, attempts were made to synthesize M-deficient phases (i.e., $Sr_3(M_{1-x}Cr_x)CrO_6$ and $Sr_3M_{1-x}CrO_{6-(3/2)x}$, vide infra) due to a deviation from full occupancy observed for the metal cation on this site, since the SrM_2O_4 could possibly arise from excess M in the reaction. All such reactions yielded approximately the same concentration of SrM_2O_4 as did the stoichiometric reactions. Notwithstanding the presence of a minor phase (except for M = Sc and In) that is more structurally complex than the major phase (lower symmetry, more parameters to refine), the refinements were good enough to determine relative phase concentrations and M (Y and rare-earth) site occupation factors for Sr_3MCrO_6. A representative X-ray powder diffraction pattern with difference plot (observed − calculated) is shown in Figure 1, for Sr_3TmCrO_6. Tick marks correspond to the allowed Bragg reflection positions for Sr_3TmCrO_6 (lower set) and for $SrTm_2O_4$ (upper set). Relevant crystallographic information and refinement statistics for the eight phases are given in Table 1; atomic positional parameters and isotropic thermal parameters are in Table 2, and derived bond lengths and angles are in Table 3.

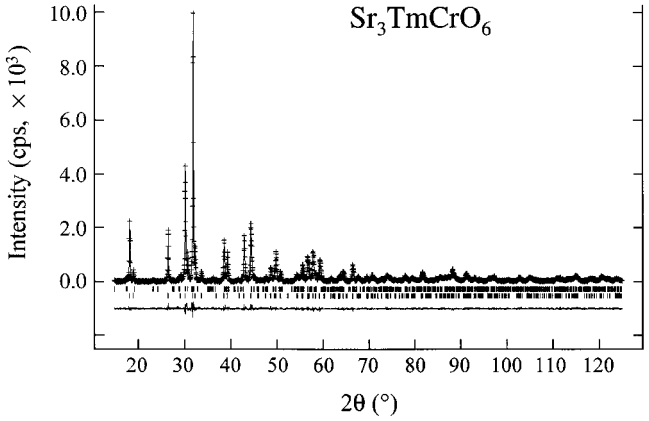

Figure 1. Experimental and calculated X-ray powder diffraction pattern of Sr_3TmCrO_6. Key: (crosses) experimental data; (solid line) Rietveld fit. Reflection markers for Sr_3TmCrO_6 (lower) and $SrTm_2O_4$ (upper) and the difference plot (observed − calculated) are shown below.

Sr_3MCrO_6 are isostructural and adopt the familiar K_4CdCl_6 structure type, consisting of $^1_\infty[MO_{6/2}CrO_{6/2}]$ chains of distorted, face-sharing metal−oxygen trigonal prisms and octahedra surrounded by chains of Sr^{2+} cations. The chains run along [001]. In all cases, the

Table 3. Selected Bond Distances (Å), Trigonal Prism Twist Angles (ϕ, °) and Octahedron O—M—O Elongation Angles (α,°)

		M							
		Sc	In	Lu	Yb	Tm	Er	Ho	Y
M—O:	6x	2.135(2)	2.217(3)	2.224(4)	2.225(4)	2.229(4)	2.251(5)	2.262(4)	2.246(4)
Cr—O:	6x	1.996(2)	2.022(3)	2.036(4)	2.024(4)	2.028(4)	2.036(4)	2.023(4)	2.022(4)
Sr—O:	2x	2.496(2)	2.502(3)	2.507(4)	2.525(4)	2.525(4)	2.525(4)	2.542(4)	2.541(4)
	2x	2.662(2)	2.634(3)	2.646(4)	2.650(4)	2.650(5)	2.639(5)	2.631(4)	2.647(4)
	2x	2.675(2)	2.649(3)	2.680(5)	2.673(5)	2.677(5)	2.686(5)	2.660(5)	2.674(4)
	2x	2.719(2)	2.733(3)	2.728(5)	2.733(5)	2.728(5)	2.721(5)	2.745(5)	2.734(5)
ϕ		11.8(1)	13.2(1)	12.3(1)	12.5(2)	12.2(2)	11.7(2)	13.4(2)	12.5(2)
α		95.6(1)	93.8(1)	93.8(1)	94.0(2)	93.5(2)	93.3(2)	93.0(2)	93.2(2)

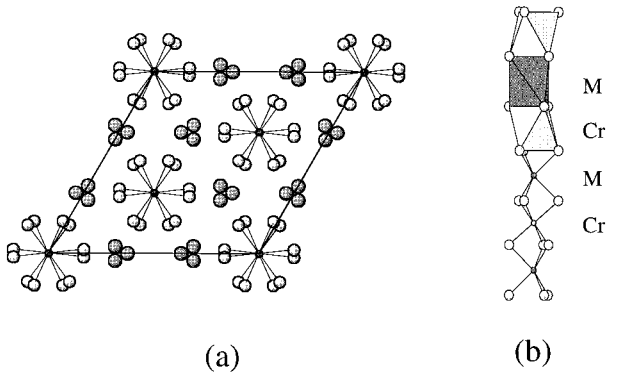

Figure 2. (a) A [001] projection of the Sr_3MCrO_6 structure. Key: (small dark circles) superimposed M and Cr atoms; (large open circles), oxygen atoms; (large dark circles) Sr atoms. (b) Off-[110] combined polyhedral and ball-and-stick view of a $^1_\infty[MO_{6/2}CrO_{6/2}]$ chain. Dark gray represents $MO_{6/2}$ trigonal prisms or M atoms, and light gray represents $CrO_{6/2}$ octahedra or Cr atoms.

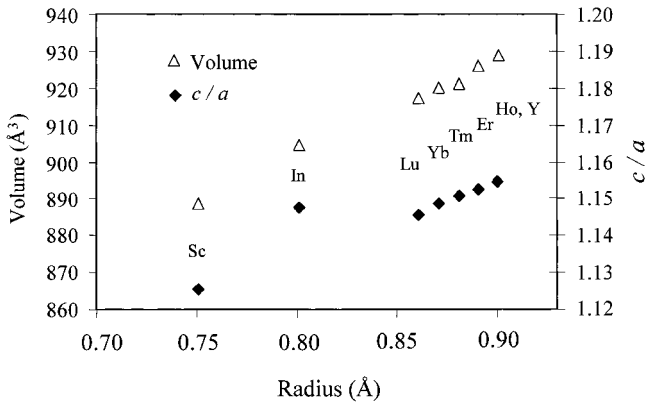

Figure 3. Unit cell volumes and *c*/*a* ratios versus M^{3+} radius for Sr_3MCrO_6.

rare-earth, Y, Sc, or In atoms were the major occupants of the trigonal prismatic site, and the chromium atom fully occupied the octahedral site. The M—O bond distances (Table 3) for the series are in the range 2.135(2)—2.262(4) Å, similar to those found in other $A_3A'BO_6$ oxides with the respective M atoms on the trigonal prismatic site.[11,12] The Cr—O distances (1.996(2)—2.036(4) Å) are typical of octahedral Cr^{3+} in an oxide matrix. Neither type of metal—oxygen polyhedron is perfectly regular. The opposite triangular faces of the "trigonal prisms" are rotated with respect to one another, producing a twist angle, ϕ. The "octahedra" are elongated along [001], resulting in one O—M—O bond angle with $\alpha > 90°$. Derived twist angles (ϕ) and O—M—O angles (α) are listed in Table 3. The metal—oxygen polyhedra adopt a strictly alternating (...octahedron-prism...) sequence, and share faces along the chain direction. Each $^1_\infty[MO_{6/2}CrO_{6/2}]$ chain is surrounded by six $^1_\infty[Sr^{2+}]$ chains; the $^1_\infty[Sr^{2+}]$ chains are in turn surrounded by three $^1_\infty[MO_{6/2}CrO_{6/2}]$ chains. The Sr^{2+} ions sit in an irregular eight-coordinate environment, on crystallographic positions slightly off the 3-fold axis with local site symmetry C_2. A [001] projection down the chains is shown in Figure 2(a) alongside an off-[110] view of one of the constituent $^1_\infty[MO_{6/2}CrO_{6/2}]$ chains (Figure 2(b)).

For the compounds Sr_3InCrO_6 and Sr_3ScCrO_6, all crystallographic sites were fully occupied. However, during the Rietveld refinements of Sr_3MCrO_6 for M = Y, Lu, Yb, Tm, Er, and Ho, a deviation from full occupancy was observed on the trigonal prismatic (M) site. Two models can be proposed:

(1) A′-site vacancies, along with oxygen vacancies adequate to satisfy charge-balance (i.e., $Sr_3M_{1-x}CrO_{6-(3/2)x}$);

(2) Partial mixing of chromium onto the M site, with no oxygen vacancies required (i.e., $Sr_3(M_{1-x}Cr_x)CrO_6$).

A similar M-site scattering deficiency was observed in the isostructural family Sr_3MNiO_6 (M = Sc, In, Y, Lu, Yb, Tm, Er) reported by Attfield in 1994,[12] and was ascribed to mixing of the Ni^{3+} cation onto the trigonal prismatic A′ site. This model was verified by simultaneous X-ray powder diffraction and time-of-flight neutron powder diffraction study on $Sr_3(Yb_{1-x}Ni_x)NiO_6$, yielding $x = 0.13$. During the refinements of Sr_3MCrO_6, no evidence for oxygen deficiency was observed for any of the phases and, considering the many similarities of Sr_3MNiO_6 to Sr_3MCrO_6 (vide infra), model (2) was assumed and the six relevant compounds refined therewith, resulting in the final compositions reported in Table 1. To gain a satisfactory answer to this question, however, further experimental study (i.e., neutron diffraction) is needed. The dependence of the *c*/*a* ratios and unit cell volumes of Sr_3MCrO_6 on the radius of the M^{3+} cation is depicted graphically in Figure 3. The slightly anomalous *c*/*a* ratio of Sr_3InCrO_6 has precedent in the compounds Sr_3MRhO_6 (M = Sc, In, Y, Yb — Gd) and Sr_3MNiO_6, and is possibly due to effects of the filled *d* shell core of the main-group ion In^{3+}. Apparently, the volume of the trigonal prismatic site in Sr_3MCrO_6 is too small to accommodate rare earths with radii >0.91 Å, as a maximum M^{3+} radius of 0.90 Å (Ho octahedral M^{3+} radius) is accepted into the structure. Mixing of the much smaller Cr^{3+} ion onto this site to decrease the

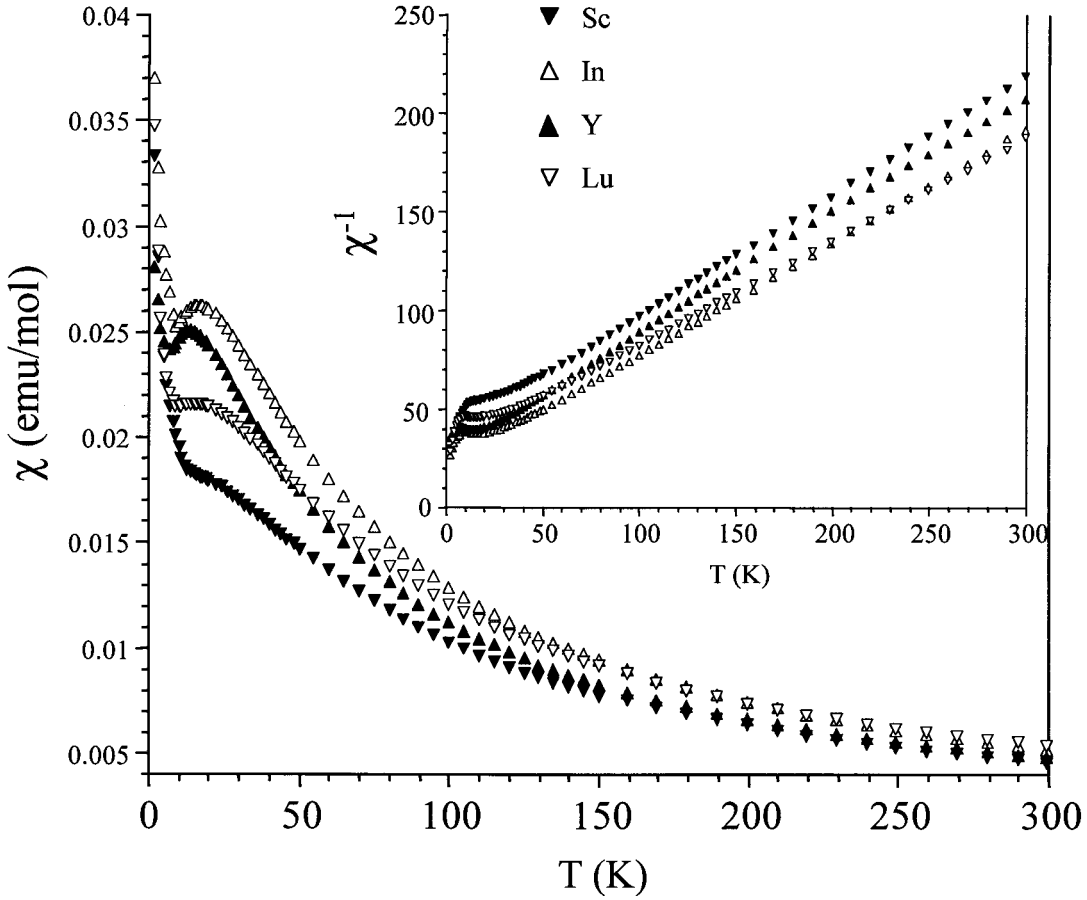

Figure 4. Magnetic susceptibility (χ, emu/mol) and inverse susceptibility (χ^{-1}, shown in the inset) as a function of temperature for M = Sc, In, Y, Lu.

average site radius also is not sufficient to stabilize this structure type for rare earths larger than holmium. The next-larger rare earth, dysprosium, has a radius only 0.01 Å greater, at 0.91 Å; however, $SrDyCrO_4$ and SrO were the only observed products from reactions involving dysprosium, even when the reactions were loaded with a deficiency of Dy (e.g., "$Sr_3Dy_{0.85}Cr_{1.15}O_6$"). The same result was found for the remaining larger rare earths, where all reactions yielded mixtures of SrO and the K_2NiF_4-type compounds $SrLnCrO_4$ (Ln = Dy, Tb, Gd, Eu, Sm, Nd, Pr, La).[35] In $SrLnCrO_4$, the rare earth and strontium atoms are statistically disordered on the spacious nine-coordinate site. It is remarkable how discriminating the radius tolerance factor for the two structure types is, as no evidence for the formation of Sr_3DyCrO_6, even as a minor phase, was found despite extended heat treatments of up to 2 weeks. On the other end of the M^{3+} size spectrum, attempts to incorporate Ga^{3+} (r = 0.62 Å) resulted in the formation of a tetragonal Ruddlesden−Popper phase (to be reported elsewhere). However, M^{3+} size effects cannot be the only factor at work in determining the formation of the $A_3A'BO_6$ structure type: reactions involving Sb^{3+}, with a six-coordinate radius of 0.76 Å, resulted in the formation of an Sb^{3+}-containing K_2NiF_4-type phase, $SrSbCrO_4$.

The structure and refinement of Sr_3MCrO_6 proceeded in many respects quite parallel to those of Sr_3MNiO_6 (though the synthetic approach was starkly different), and many of the conclusions drawn here are similar. Indeed, contrasting Sr_3MCrO_6 with the aforementioned Sr_3MNiO_6 phases is useful and interesting. Both systems involve +3/+3 pairs of cations on the A′ and B sites, in the form of a first-row transition metal on the octahedral B site, and largely the same range of elements on the trigonal prismatic A′ site. The stabilization of two slightly larger rare earths in Sr_3MCrO_6 might be correlated with the slightly larger radius of Cr^{3+} (0.615 Å) versus Ni^{3+} (0.56 Å). In Sr_3MRhO_6, where the 6-coordinate (octahedral) Rh^{3+} radius is 0.665 Å, the structure accommodates the M^{3+} rare earths up to Sm (r = 0.948 Å), providing further evidence for the trend. In both systems, the unavoidable impurity phase SrM_2O_4 was observed for the rare earth and Y compounds. Finally, in both systems, the rare earth atoms only partially occupy the trigonal prismatic M site. The most striking difference between the two systems, arising from the different electronic structures of chromium and nickel, lies with the synthetic conditions necessary to stabilize the +3 oxidation state in each case. To reach the "high" nickel oxidation state of +3, Sr_3MNiO_6 required 1 atm O_2 at 1000 °C and heating times as long as 124 h for complete reaction. Sr_3MCrO_6 presents a reverse case, where a vacuum (~0 atm O_2) was necessary to maintain the "low" oxidation state, and the reactions were finished in 24 h or less. Kinetic factors may be responsible for this difference because the chromium compounds were formed by direct reaction

(35) Joubert, J. C.; Collomb, A.; Elmaleh, D.; Le Flem, G.; Daoudi, A.; Ollivier, G. *J. Solid State Chem.* **1970**, *2*, 343.

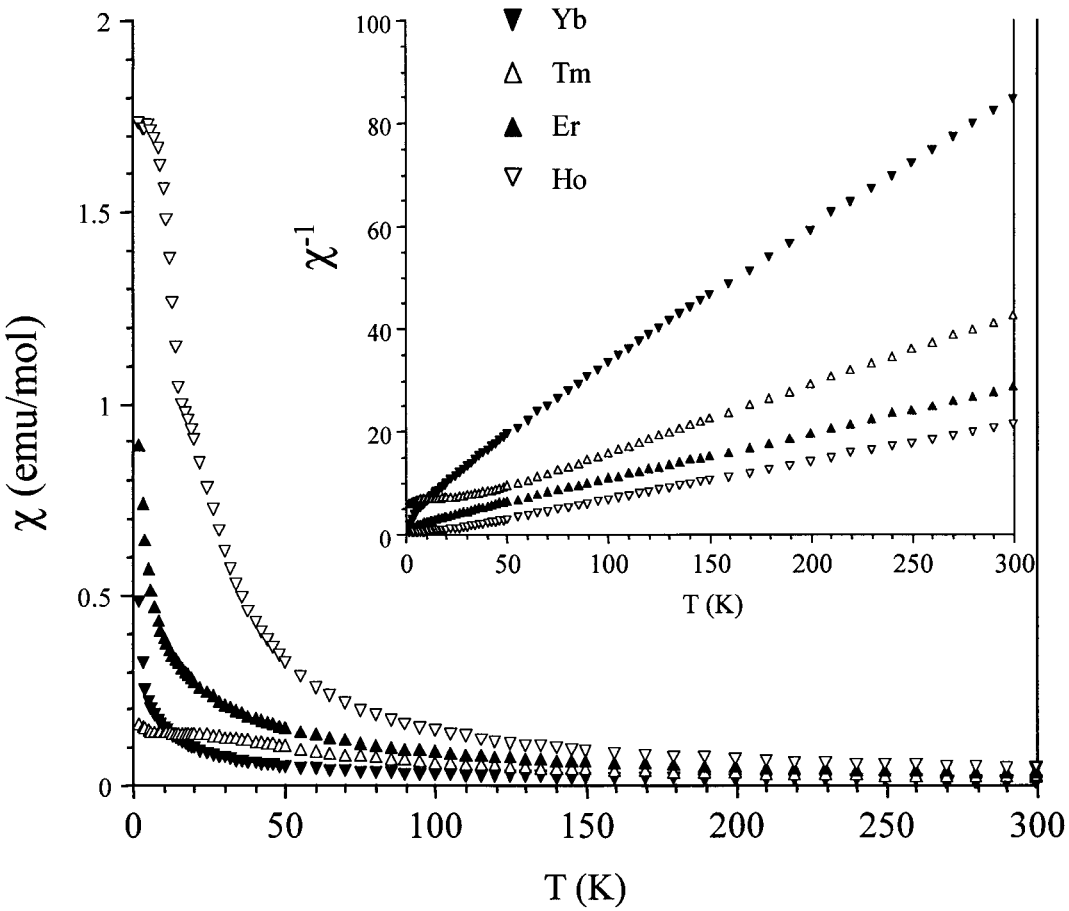

Figure 5. Magnetic susceptibility (χ, emu/mol) and inverse susceptibility (χ^{-1}, shown in the inset) as a function of temperature for M = Yb, Tm, Er, Ho.

of the binary oxides and did not require decomposition of metal carbonate or nitrate starting materials. Interestingly, the heating times necessary for complete reaction of Sr_3MNiO_6 are reported to be proportional to the M^{3+} radius, ranging from 24 h for Sr_3ScNiO_6 to 124 h for Sr_3ErNiO_6. All Sr_3MCrO_6 reactions were finished in about the same amount of time, regardless of M^{3+} radius.

Magnetic Properties. The temperature dependence of the magnetic susceptibilities of Sr_3MCrO_6 is shown in Figures 4 (M = Sc, In, Y, and Lu) and 5 (M = Yb, Tm, Er, and Ho). No history dependence of the susceptibilities was observed, as the ZFC and FC measurements overlaid exactly in each case (the ZFC data are shown in the figure). All compounds obeyed the Curie−Weiss law at higher temperatures. For all samples except M = Sc and In, the contribution to the total magnetic signal at each temperature from the impurity phases SrM_2O_4 (M = Y, Lu, Yb, Tm, Er, Ho) was subtracted. No magnetic data for these $CaFe_2O_4$-type phases are presently available in the literature; values for the susceptibilities were obtained from measurements made on pure samples prepared in this laboratory.[36] Briefly, SrM_2O_4 obey the Curie−Weiss law, with derived moments in excellent agreement with expected values. No deviations from the Curie−Weiss law were observed down to the lowest temperatures measured. All features seen in the susceptibility of the bulk samples, consequently, stem from the majority Sr_3MCrO_6 phases. It should be noted, however, that a confident analysis of the magnetic data for all phases containing the SrM_2O_4 impurity is hindered somewhat by the possibility of M/Cr mixing in the impurity phase (i.e., $SrM_{2-x}Cr_xO_4$). Unfortunately, reliable evidence for such mixing is not obtainable from the Rietveld analyses because of the low concentration of this phase in the bulk samples, but it would certainly have a noticeable effect on the measured bulk magnetism.

Figure 4 charts the molar susceptibilities and inverse molar susceptibilities versus temperature for the M = Sc, In, Y, and Lu samples. In these four systems, the metal−oxygen polyhedral chains contain a diamagnetic atom (S or $J = 0$) on the trigonal prismatic site, and Cr^{3+} (d^3, $S = 3/2$) on the octahedral site. The observed moments derived from the Curie−Weiss fit of the high-temperature data ($T > 100$ K) are consistent with three unpaired spins from Cr^{3+} (Table 4(a)). All four compounds show antiferromagnetic correlations in the Cr^{3+} sublattice, as indicated by the negative Weiss constants, and exhibit a broad maximum in the susceptibility at low temperatures, with $T(\chi_{max})$ in the range 12−25 K (Table 4(a)). The maximum in the susceptibility is most pronounced for the M = Y and In samples, broader and slightly less pronounced for M = Lu, and very broad and barely noticeable for M = Sc. At lower temperatures, a relatively large paramagnetic tail dominates the signals, which is possibly due to an impurity undetected by X-ray diffraction. The pseudo-one-dimensional nature

(36) Smith, M. D.; zur Loye, H.-C., manuscript in preparation.

Table 4. Magnetic Properties of Sr_3MCrO_6

(a) (S = 0)···(S = 3/2) chains

compound	μ_{eff}(calc)	μ_{eff}(obs)	$T(\chi_{max})$ (K)	θ (K)
Sr_3ScCrO_6	3.87	3.61	25	−59.0(4)
Sr_3InCrO_6	3.87	3.77	18	−38.7(3)
$Sr_3Y_{0.900}Cr_{1.100}O_6$	4.06	3.79	12	−56(1)
$Sr_3Lu_{0.956}Cr_{1.044}O_6$	3.95	3.90	14	−58.3(4)

(b) (J ≠ 0)···(S = 3/2) chains

compound	J	g	μ_{eff}(calc)	μ_{eff}(obs)	θ (K)
$Sr_3Yb_{0.912}Cr_{1.088}O_6$	7/2	8/7	5.92	5.56	−30.7(6)
$Sr_3Tm_{0.910}Cr_{1.090}O_6$	6	7/6	8.26	7.71	−18.9(4)
$Sr_3Er_{0.911}Cr_{1.089}O_6$	15/2	6/5	10.00	9.56	−26.8(8)
$Sr_3Ho_{0.804}Cr_{1.196}O_6$	8	5/4	10.41	10.46	4.4(4)

of these structures tempts one to assign the origin of the antiferromagnetic correlations to intrachain coupling, possibly via a superexchange pathway. However, the magnetic structures of several $A_3A'BO_6$ oxides are known to be more complex,[19, 20, 26, 37] with nonnegligible interchain interactions. Also, Carlin[38] points out that powder measurements of the susceptibility are uniformly unreliable as indicators of magnetic behavior and that additional information, such as heat capacity, is needed for a more complete characterization. Consequently, although one might be tempted to fit the data to a linear-chain $S = 3/2$ model, it is not clear that one could confidently do so given the available information.

The susceptibility versus temperature data for the remaining phases, M = Yb, Tm, Er, and Ho, where $J \neq 0$, are shown in Figure 5. Fitting the higher-temperature portion of the data ($T > 100$ K) to the Curie−Weiss law yields moments in good agreement with the expected paramagnetic contributions from Cr^{3+} and M^{3+} ions. For none of these phases is it possible to resolve any specific metal−metal interactions in the magnetic data. The temperature dependence of the M = Yb, Er, and Ho samples does not reveal any magnetic ordering down to the lowest temperature measured (2 K). Parameters derived from the fit are given in Table 4(b). The Weiss constants are negative for the M = Yb and Er samples, suggesting that antiferromagnetic correlations might take place in these compounds as well. The Weiss constant for M = Ho, on the other hand, is slightly positive. The M = Tm sample shows evidence of weak magnetic correlations, in the form of a slight antiferromagnetic-like decrease in the susceptibility centered near $T = 15$ K. However, because the deviation from the Curie−Weiss behavior is very small and because $SrTm_2O_4$ is present as an impurity, it is not possible to identify the origin of this deviation.

(37) Lee, K.-S.; Koo, H.-J.; Whangbo, M.-H. *Inorg. Chem.* **1999**, *38*, 2199.

(38) Carlin, R. L. *Magnetochemistry*; Springer-Verlag: Berlin, 1986; Chapter 7.

Conclusions

We have succeeded in incorporating Cr^{3+} into the $A_3A'BO_6$ structural family by in vacuo synthesis using constituent oxides. Sr_3MCrO_6 formed quite readily for M^{3+} = Sc, In, Y, Lu, Yb, Tm, Er, and Ho, but M^{3+} ions larger the Ho^{3+} ($r = 0.90$ Å) yielded other products. The ease with which Sr_3MCrO_6 formed under the right (anaerobic) conditions gives encouragement for similar preparations of other $A_3A'BO_6$ phases containing "reduced" ions, such as V^{3+} or V^{4+}, Mo^{4+}, and Os^{4+}, and the opportunity to study the magnetic properties of such unusual oxides. Sr_3MCrO_6 adopt the expected pseudo-one-dimensional K_4CdCl_6 structure type, containing infinite chains of $MO_{6/2}$ trigonal prisms and $CrO_{6/2}$ octahedra that share faces. The M^{3+} trigonal prismatic site was substituted by a small percentage (4−20%) of chromium in the M = Y, Lu, Yb, Tm, Er, and Ho samples. The compounds were found to obey the Curie−Weiss law, with observed moments consistent with noninteracting M^{3+} and Cr^{3+} centers.

Acknowledgment. Funding for this research was provided by the National Science Foundation through Grant No. DMR:9873570. Research was carried out in part at the National Synchrotron Light Source, Brookhaven National Laboratory, which is supported by the US Department of Energy, Division of Materials Science and Division of Chemical Sciences. We thank Dr. D. E. Cox for assistance in collecting the data, and Dr. Kara Beauchamp for helpful discussions.

CM000084A